

UNIVERSITY OF WATERLOO  
Faculty of Science

*Kinetic density from ab initio theory*

Theory Group - TRIUMF  
Vancouver, British Columbia

prepared by

Michael Gennari  
#20552297  
4A Mathematical Physics  
September 2018

1330 Burrard Street  
Vancouver, BC  
V6Z 2B7

September 10, 2018

Brian McNamara  
Physics and Astronomy  
University of Waterloo  
Waterloo, Ontario  
V6T 2A3

Dear Brian McNamara,

I have prepared the enclosed report “Kinetic density from *ab initio* theory” as my 4A Work Report for TRIUMF. This completed and verified work, the fourth and final work report that Co-operative Education Program requires that I complete as part of my Co-op BSc degree requirements, has not received previous academic credit.

The Theory Group at TRIUMF, led by my supervisor Petr Navrátil, focuses on *ab initio* approaches to theories in nuclear and particle physics. As a researcher in theoretical nuclear physics at TRIUMF, I assisted Dr. Petr Navrátil in developing translationally invariant nonlocal one-body densities, which have allowed us to apply the no-core shell model and compare results with different many-body techniques in nuclear theory. The results presented in this work report are currently under review for publishing, and can be found on arXiv:1808.10537.

This report was written entirely by myself and has not received previous academic credit at any institution. I would like to thank Dr. Petr Navrátil and Dr. Angelo Calci for assisting and guiding me with my work throughout the past several terms at TRIUMF. I give permission to TRIUMF to keep this report on file and use it for internal reporting and external reporting including publication.

Sincerely,

Michael Gennari

Encl.

## Kinetic density from *ab initio* theory

The kinetic density, a fundamental quantity of density functional theory (DFT), is analytically computed from the *ab initio* no-core shell model (NCSM), using the nonlocal scalar one-body nuclear densities. The NCSM takes two- and three-nucleon chiral interactions as the sole input. One can directly gauge the impact of the spurious center-of-mass (COM) contributions in the nuclear density by comparing the kinetic density results from translationally invariant and COM contaminated densities. The nonlocal density is a second quantization object derived from the NCSM one-body densities. We review the generation of translationally invariant densities and proceed to present an analytic method for computing the kinetic density from *ab initio* theory. This method is generalizable to other quantities in DFT. The nonlocal densities of  $^{4,6,8}\text{He}$ ,  $^{12}\text{C}$ , and  $^{16}\text{O}$  are computed in the NCSM and are then used to compute the nuclear kinetic density. We discuss the impact of COM removal in the density. We show that it is possible to compute fundamental objects in DFT from *ab initio* models, allowing for the benchmarking of COM removal techniques across varying many-body techniques.

# Contents

<b>1.0 Introduction</b> . . . . .	<b>1</b>
<b>2.0 Theoretical framework</b> . . . . .	<b>3</b>
2.1 No-core shell model (NCSM) . . . . .	3
2.2 Nonlocal density . . . . .	4
2.3 Kinetic density . . . . .	7
2.3.1 Derivative of radial harmonic oscillator (RHO) function	8
2.3.2 Derivation of kinetic density . . . . .	9
<b>3.0 Analysis</b> . . . . .	<b>12</b>
3.1 Review of nonlocal density results . . . . .	12
3.2 Kinetic density results . . . . .	19
3.3 Comparison to basic DFT calculation . . . . .	26
<b>4.0 Conclusions</b> . . . . .	<b>29</b>
<b>5.0 Recommendations</b> . . . . .	<b>30</b>
<b>6.0 Appendix</b> . . . . .	<b>30</b>
6.1 Kinetic density coefficients . . . . .	30
<b>7.0 Acknowledgments</b> . . . . .	<b>33</b>

## List of Figures

- Fig. 1 — Ground state  $^4\text{He}$  nonlocal proton and neutron densities calculated using the bare NN-N<sup>4</sup>LO(500) interaction with an  $N_{\max} = 18$  basis space. An oscillator frequency of  $\hbar\Omega = 20.0$  MeV was used for this calculation. . . . . 13
- Fig. 2 — Ground state  $^4\text{He}$  nonlocal proton and neutron densities calculated using the SRG-evolved NN-N<sup>4</sup>LO(500)+3Nlnl interaction with an  $N_{\max} = 14$  basis space. An oscillator frequency of  $\hbar\Omega = 20.0$  MeV and a flow parameter of  $\lambda_{\text{SRG}} = 2.0$  fm<sup>-1</sup> were used for the calculations. . . . . 13
- Fig. 3 — Ground state *trinv* local density comparison for  $^4\text{He}$ . In the top panel are calculations with two-body (NN+3Nind SRG) and two- plus three-body (NN+3N SRG) SRG-evolved interactions, while in the bottom panel we have the bare two-body NN-N<sup>4</sup>LO(500) interaction. . . . . 13
- Fig. 4 — Ground state  $^6\text{He}$  nonlocal proton and neutron densities calculated using the NN-N<sup>4</sup>LO(500)+3Nlnl interaction with an  $N_{\max} = 12$  basis space. An oscillator frequency of  $\hbar\Omega = 20.0$  MeV and a flow parameter of  $\lambda_{\text{SRG}} = 2.0$  fm<sup>-1</sup> were used for the calculations. . . . . 15
- Fig. 5 — Ground state  $^8\text{He}$  nonlocal proton and neutron densities calculated using the NN-N<sup>4</sup>LO(500)+3Nlnl interaction with an  $N_{\max} = 10$  basis space. An oscillator frequency of  $\hbar\Omega = 20.0$  MeV and a flow parameter of  $\lambda_{\text{SRG}} = 2.0$  fm<sup>-1</sup> were used for the calculations. . . . . 15

Fig. 6 —	Ground state $^{12}\text{C}$ nonlocal proton and neutron densities computed using the NN-N $^4\text{LO}(500)$ +3Nlnl interaction with an $N_{\max} = 8$ importance truncated basis space, an oscillator frequency of $\hbar\Omega = 20.0$ MeV, and a flow parameter of $\lambda_{\text{SRG}} = 1.8 \text{ fm}^{-1}$ . . . . .	16
Fig. 7 —	Ground state $^{16}\text{O}$ nonlocal proton and neutron densities computed using the NN-N $^4\text{LO}(500)$ +3Nlnl interaction with an $N_{\max} = 8$ importance truncated basis space, an oscillator frequency of $\hbar\Omega = 20.0$ MeV, and a flow parameter of $\lambda_{\text{SRG}} = 1.8 \text{ fm}^{-1}$ . . . . .	16
Fig. 8 —	Ground state $^4\text{He}$ local proton and neutron densities computed using the NN-N $^4\text{LO}(500)$ +3Nlnl interaction with an $N_{\max} = 14$ basis space, an oscillator frequency of $\hbar\Omega = 20.0$ MeV, and a flow parameter of $\lambda_{\text{SRG}} = 2.0 \text{ fm}^{-1}$ . . . . .	17
Fig. 9 —	Ground state $^6\text{He}$ local proton and neutron densities computed using the NN-N $^4\text{LO}(500)$ +3Nlnl interaction with an $N_{\max} = 12$ basis space, an oscillator frequency of $\hbar\Omega = 20.0$ MeV, and a flow parameter of $\lambda_{\text{SRG}} = 2.0 \text{ fm}^{-1}$ . . . . .	17
Fig. 10 —	Ground state $^8\text{He}$ local proton and neutron densities computed using the NN-N $^4\text{LO}(500)$ +3Nlnl interaction with an $N_{\max} = 10$ basis space, an oscillator frequency of $\hbar\Omega = 20.0$ MeV, and a flow parameter of $\lambda_{\text{SRG}} = 2.0 \text{ fm}^{-1}$ . . . . .	18

Fig. 11 — Ground state $^{12}\text{C}$ local proton and neutron densities computed using the NN-N <sup>4</sup> LO(500)+3Nlnl interaction with an $N_{\max} = 10$ basis space, an oscillator frequency of $\hbar\Omega = 20.0$ MeV, and a flow parameter of $\lambda_{\text{SRG}} = 2.0 \text{ fm}^{-1}$ . . . . .	18
Fig. 12 — Ground state $^{16}\text{O}$ local proton and neutron densities computed using the NN-N <sup>4</sup> LO(500)+3Nlnl interaction with an $N_{\max} = 10$ basis space, an oscillator frequency of $\hbar\Omega = 20.0$ MeV, and a flow parameter of $\lambda_{\text{SRG}} = 2.0 \text{ fm}^{-1}$ . . . . .	19
Fig. 13 — Ground state <i>trinv</i> kinetic density comparison for $^4\text{He}$ . In the top panel are calculations with two-body (NN+3Nind SRG) and two- plus three-body (NN+3N SRG) SRG-evolved interactions, while in the bottom panel we have the bare two-body NN-N <sup>4</sup> LO(500) interaction. Nonlocal densities were computed as previously described in Fig. 1 and Fig. 2, respectively. . . . .	20
Fig. 14 — Ground state $^4\text{He}$ comparisons between the <i>trinv</i> and <i>wiCOM</i> kinetic densities. The nonlocal density was computed as previously described in Sec. 3.1. The expectation value of the intrinsic kinetic energy for $^4\text{He}$ is 51.91 MeV. . . . .	21
Fig. 15 — Ground state $^6\text{He}$ comparisons between the <i>trinv</i> and <i>wiCOM</i> kinetic densities. The nonlocal density was computed as previously described in Sec. 3.1. The expectation value of the intrinsic kinetic energy for $^6\text{He}$ is 78.26 MeV. . . . .	22

Fig. 16 — Ground state $^8\text{He}$ comparisons between the <i>trinv</i> and <i>wiCOM</i> kinetic densities. The nonlocal density was computed as previously described in Sec. 3.1. The expectation value of the intrinsic kinetic energy for $^8\text{He}$ is 116.30 MeV. . . . .	22
Fig. 17 — Ground state $^{12}\text{C}$ comparisons between the <i>trinv</i> and <i>wiCOM</i> kinetic densities. The nonlocal density was computed as previously described in Sec. 3.1. The expectation value of the intrinsic kinetic energy for $^{12}\text{C}$ is 219.84 MeV. . . . .	23
Fig. 18 — Ground state $^{16}\text{O}$ comparisons between the <i>trinv</i> and <i>wiCOM</i> kinetic densities. The nonlocal density was computed as previously described in Sec. 3.1. The expectation value of the intrinsic kinetic energy for $^{16}\text{O}$ is 301.69 MeV. . . . .	24
Fig. 19 — Ground state kinetic density results for $^{4,8}\text{He}$ , $^{12}\text{C}$ , and $^{16}\text{O}$ calculated with the NN-N <sup>4</sup> LO(500)+3Nlnl interaction. The nonlocal densities for the nuclei were computed as previously described in Sec. 3.1. The DFT kinetic density was obtained by using Eq. (29), $\tau_{DFT}(r) = (1 - \frac{1}{A})\tau_{wiCOM}(r)$ . . . . .	27

## List of Tables

Table 1 —	Ground state mean intrinsic kinetic energy values and percent errors for all aforementioned nuclei calculated using the NN-N <sup>4</sup> LO(500)+3Nlnl interaction (except <sup>4</sup> Hebare, which are the results for the bare NN-N <sup>4</sup> LO(500) interaction). All $\langle T_{int} \rangle$ values are in MeV. Note <i>IT</i> refers to an importance truncated basis space. Error is calculated using the percent difference between the maximum $N_{\max}$ value and the previous value. . . . . . . . . . .	25
Table 2 —	Ground state mean intrinsic kinetic energy values using <i>trinv</i> , <i>wiCOM</i> , and DFT kinetic densities for all aforementioned nuclei, calculated with the NN-N <sup>4</sup> LO(500)+3Nlnl interaction. All $\langle T_i \rangle$ values are in MeV. Note <i>IT</i> refers to an importance truncated basis space. The $\langle T_{DFT} \rangle$ is calculated by using Eq. (29), $\langle T_{DFT} \rangle = (1 - \frac{1}{A}) \langle T_{wiCOM} \rangle$ .	28

## 1.0 Introduction

In this work, we provide an analytic approach for computing the kinetic density of a nucleus from the nonlocal scalar one-body densities, using the method previously introduced in Ref. [1]. The microscopic nonlocal density is constructed from the one-body density matrix elements generated in second quantization, computed within the no-core shell model (NCSM) [2]. The NCSM is an *ab initio* many-body technique which treats each nucleon as an individual degree of freedom, taking only two- and three-nucleon interactions as input for calculation. The NCSM is well suited for the description of relatively light nuclei as it is a rigorous technique, accounting for many-nucleon correlations, which allow it to produce high-quality wave functions for *s*- and *p*-shell nuclei.

There are several fundamental quantities in density functional theory (DFT), such as the kinetic density, which were previously inaccessible using *ab initio* approaches. Using the NCSM nonlocal densities, we are capable of computing the kinetic density from our high-quality wave functions. In larger systems ( $A \approx 16$ ) where DFT is better suited for describing nuclear properties, we can make direct comparison between COM removal techniques across different many-body methods. In particular, we compare to a simple DFT calculation. DFT is a many-body technique which has been practiced for approximately 40 years, and is particularly adept at calculating nuclear properties across a wide section of the nuclear chart [3, 4, 5, 6, 7, 8, 9]. In DFT, an energy functional is constructed from system densities (kinetic, spin, isospin, etc.) and is minimized to give access to nuclear properties. This technique has had wide success and has been able to make strides in the description heavier nuclear systems [10, 11, 12, 13, 14]. In heavier systems,

one finds reduced effects from nonlocality and center-of-mass (COM) contamination, however if DFT is to attempt to describe lighter systems, the behavior of these effects in DFT must be examined. We primarily discuss results for  $^{16}\text{O}$  using the NCSM many-body technique so that we may gauge potential contamination of the COM in the kinetic density.

In Sec. 2.0 , we discuss the construction of the nuclear and kinetic densities from *ab initio* theory, including derivations. In Sec. 3.0 , we review results for the density, we discuss kinetic density results, and we make a comparison between the translationally invariant and COM contaminated kinetic density. In Sec. 4.0 , we draw our conclusions. In Sec. 5.0 , we provide our recommendations. Sec. 6.0 contains coefficients necessary to the calculation of the kinetic density.

## 2.0 Theoretical framework

### 2.1 No-core shell model (NCSM)

In order to compute the kinetic density from an *ab initio* nonlocal one-body density, we require knowledge of the NCSM wave functions. The NCSM produces the required  $A$ -nucleon eigenstates by considering nuclei to be nonrelativistic systems of  $A$  point-like particles – each treated as an individual degree of freedom – interacting via controlled, high-precision two- and three-body inter-nucleon interactions [2]. The angular momentum, parity, and translational invariance of observables are conserved for the nucleus being considered. The NCSM eigenstates are expanded over a set of antisymmetric  $A$ -nucleon harmonic oscillator (HO) states characterized by the frequency of the HO well  $\Omega$ , containing  $N_{\max}$  HO shells higher than the lowest Pauli configuration. Additional information on the NCSM can be found in Ref. [2].

The NCSM eigenstates are calculated via diagonalization of the nuclear Hamiltonian generated from two- and three-nucleon (NN+3N) interactions:

$$\hat{H} |A\lambda J^\pi T\rangle = E_\lambda^{J^\pi T} |A\lambda J^\pi T\rangle , \quad (1)$$

with  $\lambda$  being used to distinguish eigenstates with identical  $J^\pi T$ .

The convergence of the HO expansion can be, in general, accelerated by use of a similarity renormalization group (SRG) being applied to the NN and 3N potentials, characterized by the momentum-decoupling scale,  $\lambda_{\text{SRG}}$  [15, 16, 17, 18, 19]. Significant gains can be achieved with the SRG

evolutions, however it induces higher body terms and has the potential to introduce a further dependence on the momentum-decoupling scale if unitarity of the transformation is violated.

Throughout working with the kinetic densities, we chose to use the fifth order NN chiral potential order ( $N^4LO$ ) with a momentum cutoff of  $\Lambda = 500$  MeV [20, 21]. The two-body portion of our interaction will be labeled NN- $N^4LO(500)$ . In addition, we include the three-nucleon potential at third order ( $N^2LO$ ) with simultaneous local [22] and nonlocal regularization. See Ref. [1] for additional information on the regularization. The three-body component of the interaction will be labeled 3Nlnl. Our total interaction is this NN- $N^4LO(500)$ +3Nlnl. Note that calculations involving both  $^{12}C$  and  $^{16}O$  were performed using importance truncated NCSM basis spaces [23, 24].

## 2.2 Nonlocal density

We make use of the Jacobi coordinate space COM removal technique established in Ref. [1] to compute translationally invariant nonlocal one-body density matrices. This is a generalized form of the results of Ref. [25]. The operator form of the density is as follows,

$$\rho_{op}(\vec{r}, \vec{r}') = \sum_{i=1}^A (|\vec{r}\rangle\langle\vec{r}'|)^i = \sum_{i=1}^A \delta(\vec{r} - \vec{r}_i)\delta(\vec{r}' - \vec{r}'_i). \quad (2)$$

Expressing our NCSM eigenstates – with subscript  $SD$  as an identifier – in the Cartesian coordinate single particle slater-determinant (SD) basis and

computing the the matrix element of the operator, we find that

$$\begin{aligned}
& {}_{SD} \langle A\lambda_j J_j M_j | \rho_{op}(\vec{r}, \vec{r}') | A\lambda_i J_i M_i \rangle_{SD} \\
&= \sum \frac{1}{\hat{J}_f} (J_i M_i K k | J_f M_f) \left( Y_{l_1}^*(\hat{r}) Y_{l_2}^*(\hat{r}') \right)_k^{(K)} \\
&\quad \times R_{n_1, l_1}(|\vec{r}|) R_{n_2, l_2}(|\vec{r}'|) \\
&\quad \times (-1)^{l_1 + l_2 + K + j_2 + \frac{1}{2}} \hat{j}_1 \hat{j}_2 \hat{K} \left\{ \begin{array}{ccc} j_2 & l_2 & \frac{1}{2} \\ l_1 & j_1 & K \end{array} \right\} \\
&\quad \times \frac{(-1)}{\hat{K}} {}_{SD} \langle A\lambda_f J_f | | (a_{n_1, l_1, j_1}^\dagger \tilde{a}_{n_2, l_2, j_2})^{(K)} | | A\lambda_i J_i \rangle_{SD}.
\end{aligned} \tag{3}$$

where we have suppressed both isospin and parity quantum numbers. The eigenstates are expressed using the SD HO basis, which includes the COM degrees-of-freedom (DOF). Additionally,  $\hat{\eta} = \sqrt{2\eta + 1}$  and  $R_{n,l}(|\vec{r}|)$  is defined as the radial harmonic oscillator (RHO) wave function, with an oscillator length parameter  $b = \sqrt{\frac{\hbar}{m\Omega}}$ , where  $m$  is the nucleon mass. Both coordinates are measured directly from the center of the harmonic oscillator potential well. The matrix elements shown are the one-body density matrix elements. The result of this construction is contamination from the COM in our nuclear density. The object of previous work was to remove the COM component from the nonlocal density, allowing for more consistent calculations of objects dependent on the nuclear density. A factorization of SD and Jacobi eigenstates allows us to decouple the ground state COM component  $\phi_{000}(\vec{\xi}_0)$  of the wave function, thus isolating the intrinsic part of the wave function:

$$\begin{aligned}
& \langle \vec{r}_1 \dots \vec{r}_A \vec{\sigma}_1 \dots \vec{\sigma}_A \vec{\tau}_1 \dots \vec{\tau}_A | A\lambda JM \rangle_{SD} = \\
& \langle \vec{\xi}_1 \dots \vec{\xi}_{A-1} \vec{\sigma}_1 \dots \vec{\sigma}_A \vec{\tau}_1 \dots \vec{\tau}_A | A\lambda JM \rangle \phi_{000}(\vec{\xi}_0),
\end{aligned} \tag{4}$$

The coordinate of the ground state COM wave function,  $\vec{\xi}_0$ , is proportional to the  $A$ -nucleon COM coordinate. Following the procedure of Ref. [1], the translationally invariant one-body density matrix elements are given by

$$\begin{aligned}
& \langle A\lambda_j J_j M_j | \rho_{op}^{trinv}(\vec{r} - \vec{R}, \vec{r}' - \vec{R}) | A\lambda_i J_i M_i \rangle \\
&= \left( \frac{A}{A-1} \right)^{\frac{3}{2}} \sum \frac{1}{J_f} (J_i M_i K k | J_f M_f) \\
&\quad \times (M^K)_{nl n' l', n_1 l_1 n_2 l_2}^{-1} \left( Y_l^*(\widehat{\vec{r} - \vec{R}}) Y_{l'}^*(\widehat{\vec{r}' - \vec{R}}) \right)_k^{(K)} \\
&\quad \times R_{n,l} \left( \sqrt{\frac{A}{A-1}} |\vec{r} - \vec{R}| \right) R_{n',l'} \left( \sqrt{\frac{A}{A-1}} |\vec{r}' - \vec{R}| \right) \\
&\quad \times (-1)^{l_1 + l_2 + K + j_2 - \frac{1}{2}} \hat{j}_1 \hat{j}_2 \left\{ \begin{array}{ccc} j_1 & j_2 & K \\ l_2 & l_1 & \frac{1}{2} \end{array} \right\} \\
&\quad \times {}_{SD} \langle A\lambda_f J_f | (a_{n_1, l_1, j_1}^\dagger \tilde{a}_{n_2, l_2, j_2})^{(K)} | A\lambda_i J_i \rangle_{SD}
\end{aligned} \tag{5}$$

where

$$\begin{aligned}
& (M^K)_{nl n' l', n_1 l_1 n_2 l_2} \\
&= \sum_{N_1, L_1} (-1)^{l+l'+K+L_1} \left\{ \begin{array}{ccc} l_1 & L_1 & l \\ l' & K & l_2 \end{array} \right\} \hat{l} \hat{l}' \\
&\quad \times \langle nl00l | N_1 L_1 n_1 l_1 l \rangle_{\frac{1}{A-1}} \langle n'l'00l' | N_1 L_1 n_2 l_2 l' \rangle_{\frac{1}{A-1}} .
\end{aligned} \tag{6}$$

We again note the RHO functions,  $R_{n,l} \left( \sqrt{\frac{A}{A-1}} |\vec{r} - \vec{R}| \right)$ , the argument of which is a relative Jacobi coordinate  $\vec{\xi} = -\sqrt{\frac{A}{A-1}} (\vec{r} - \vec{R})$ . Our coordinate is now measured from the center of the HO well. The matrix labeled as

$(M^K)_{nl n' l', n_1 l_1 n_2 l_2}$ , originally introduced in Ref. [25], contains generalized HO brackets describing a two particle system with a mass ratio of  $d$ , as described in Ref. [26]. Note that proton and neutron densities are obtained separately by inclusion of  $(\frac{1}{2} \pm t_{zi})$  factors in Eq. (2).

Our densities are normalized according to the standard in Ref. [25], such that the integral of the local density ( $\vec{r} = \vec{r}'$ )

$$\int d\vec{r} \langle A\lambda JM | \rho_{op}(\vec{r}, \vec{r}) | A\lambda JM \rangle = A \quad (7)$$

gives the corresponding number of nucleons for both (3) and (5). The normalization in Eq. (7) then becomes  $Z$  or  $N$  for the proton and neutron density respectively.

### 2.3 Kinetic density

DFT has several fundamental, non-observable density objects which are used as input in local energy density functionals  $E(\rho)$ . These functionals are then minimized to obtain nuclear properties. The kinetic density is but one of these densities, which is taken as an input along with nuclear interaction terms to the local energy density  $\mathcal{H}(\vec{r})$ , which is a true observable [27]. The kinetic contribution in the local energy density is given by

$$\mathcal{H}_{kinetic}(\vec{r}) = \frac{\hbar^2}{2m} \tau_0(\vec{r}), \quad (8)$$

where  $m$  is the nucleon mass and  $\tau_0 = \tau_p + \tau_n$  is the total kinetic density [28]. With the construction of the *ab initio* nonlocal nuclear densities, it is possible to derive an analytic expression for the kinetic density in terms of the one-body density matrix elements by use of the following relation:

$$\tau_{\mathcal{N}}(\vec{r}) = \left[ \vec{\nabla} \cdot \vec{\nabla}' \rho_{\mathcal{N}}(\vec{r}, \vec{r}') \right]_{\vec{r}=\vec{r}'} . \quad (9)$$

where  $\mathcal{N}$  denotes the nucleon type – protons ( $p$ ) and neutrons ( $n$ ).

### 2.3.1 Derivative of radial harmonic oscillator (RHO) function

We begin by first introducing existing derivative and recurrence relations for Laguerre polynomials:

$$\frac{d}{dr} L_n^l(r) = -L_{n-1}^{l+1}(r) \quad (10)$$

$$L_n^l(r) + L_{n-1}^{l+1}(r) = L_n^{l+1}(r) \quad (11)$$

We also remind the reader of the form of the RHO,

$$R_{n,l}(r) = \sqrt{\frac{2\Gamma(n+1)}{(b^2)^{l+\frac{3}{2}}\Gamma(n+l+\frac{3}{2})}} r^l \exp\left(-\frac{r^2}{2b^2}\right) L_n^{l+\frac{1}{2}}\left(\frac{r^2}{b^2}\right), \quad (12)$$

where  $b$  is the harmonic oscillator length and  $\Gamma$  is the gamma function. We make the following definition for simplicity,

$$\gamma_{n,l,b} = \sqrt{\frac{2\Gamma(n+1)}{(b^2)^{l+\frac{3}{2}}\Gamma(n+l+\frac{3}{2})}}. \quad (13)$$

By taking the radial derivative on the RHO function, and making us of Eq. (10), we have

$$\begin{aligned} \frac{dR_{n,l}}{dr} &= \gamma_{n,l,b} \left[ lr^{l-1} \exp\left(-\frac{r^2}{2b^2}\right) L_n^{l+\frac{1}{2}}\left(\frac{r^2}{b^2}\right) - \frac{r^{l+1}}{b^2} \exp\left(-\frac{r^2}{2b^2}\right) L_n^{l+\frac{1}{2}}\left(\frac{r^2}{b^2}\right) \right. \\ &\quad \left. - \frac{2r^{l+1}}{b^2} \exp\left(-\frac{r^2}{2b^2}\right) L_{n-1}^{l+\frac{3}{2}}\left(\frac{r^2}{b^2}\right) \right]. \end{aligned} \quad (14)$$

If we then utilize Eq. (11) and write our expression in terms of RHO functions,

$$\begin{aligned}\frac{dR_{n,l}}{dr} &= \frac{l}{r}R_{n,l}(r) - \gamma_{n,l,b}\frac{r^{l+1}}{b^2}\exp\left(-\frac{r^2}{2b^2}\right)\left[L_n^{l+\frac{1}{2}}\left(\frac{r^2}{b^2}\right) + 2L_{n-1}^{l+\frac{3}{2}}\left(\frac{r^2}{b^2}\right)\right] \\ \frac{dR_{n,l}}{dr} &= \frac{l}{r}R_{n,l}(r) - \gamma_{n,l,b}\frac{r^{l+1}}{b^2}\exp\left(-\frac{r^2}{2b^2}\right)\left[L_n^{l+\frac{3}{2}}\left(\frac{r^2}{b^2}\right) + L_{n-1}^{l+\frac{3}{2}}\left(\frac{r^2}{b^2}\right)\right] \\ \frac{dR_{n,l}}{dr} &= \frac{l}{r}R_{n,l}(r) - \frac{1}{b^2}\gamma_{n,l,b}\left[\frac{R_n^{l+1}(r)}{\gamma_{n,l+1,b}} + \frac{R_{n-1}^{l+1}(r)}{\gamma_{n-1,l+1,b}}\right]\end{aligned}\quad (15)$$

we arrive at our final result,

$$\frac{dR_{n,l}}{dr} = \frac{l}{r}R_{n,l} - \frac{1}{b}\left[\sqrt{n+l+\frac{3}{2}}R_{n,l+1}(r) + \sqrt{n}R_{n-1,l+1}(r)\right]\quad (16)$$

### 2.3.2 Derivation of kinetic density

Here we start from Eq. (9), where the kinetic density is dependent on the nonlocal nuclear density. We then expand using the following relation

$$\vec{\nabla} \cdot \vec{\nabla}' = \sum_{\mu=\pm 1,0} (-1)^{\mu} \nabla_{\mu} \nabla'_{-\mu}.\quad (17)$$

and so

$$\tau_{\mathcal{N}}(\vec{r}) = \left[ \nabla_0 \nabla'_0 \rho_{\mathcal{N}}(\vec{r}, \vec{r}') - \nabla_{+1} \nabla'_{-1} \rho_{\mathcal{N}}(\vec{r}, \vec{r}') - \nabla_{-1} \nabla'_{+1} \rho_{\mathcal{N}}(\vec{r}, \vec{r}') \right]_{\vec{r}=\vec{r}'}.\quad (18)$$

We then note that the individual terms in this expression may be written in a more compact form, with the density coefficients absorbed into a singular

coefficient  $\alpha$  as is done in Eq. (19)

$$\begin{aligned} \nabla_u \nabla'_{-u} \rho(\vec{r}, \vec{r}') = & \sum_{n,l,n',l',K,k,m_l,m_{l'}} \alpha_{n,l,n',l'}^{K,i,f} (l m_l l' m_{l'} | LM) \\ & \times \left[ \nabla_u R_{n,l}(r) Y_{l,m_l}^*(\hat{r}) \right] \left[ \nabla'_{-u} R_{n',l'}(r') Y_{l',m_{l'}}^*(\hat{r}') \right] , \end{aligned} \quad (19)$$

where  $u = 0, \pm 1$  and  $\alpha_{n,l,n',l'}^{K,i,f}$  is defined for the translationally invariant density as

$$\begin{aligned} \alpha_{n,l,n',l'}^{K,i,f} = & \sum_{n_1,l_1,j_1,n_2,l_2,j_2} \left( \frac{A}{A-1} \right)^{3/2} \\ & \times \frac{1}{\hat{J}_f} (J_i M_i K k | J_f M_f) (M^K)_{n,l,n',l',n_1,l_1,n_2,l_2}^{-1} \\ & \times (-1)^{l_1+l_2+K+j_2-\frac{1}{2}} \hat{j}_1 \hat{j}_2 \left\{ \begin{array}{ccc} j_1 & j_2 & K \\ l_2 & l_1 & \frac{1}{2} \end{array} \right\} \\ & \times {}_{SD} \langle A \lambda_f J_f | (a_{n_1,l_1,j_1}^\dagger \tilde{a}_{n_2,l_2,j_2})^{(K)} | A \lambda_i J_i \rangle_{SD} . \end{aligned} \quad (20)$$

Of course, we note that as the angular momentum algebra is different for the translationally invariant and COM contaminated nuclear densities, as are the expressions for  $\alpha$ . As the method is general and can be applied to all terms, let us now only consider the  $\nabla_0 \nabla'_0 \rho_N(\vec{r}, \vec{r}')|_{\vec{r}=\vec{r}'}$  component, since the angular momentum algebra is less intensive. Additionally, we suppress the  $N$  isospin label since the procedure is identical for protons and neutrons. It is then convenient to write

$$\begin{aligned} \nabla_0 \nabla'_0 \rho(\vec{r}, \vec{r}')|_{\vec{r}=\vec{r}'} = & \sum_{n,l,n',l',K,k,m_l,m_{l'}} \alpha_{n,l,n',l'}^{K,i,f} (l m_l l' m_{l'} | LM) \\ & \times \left[ \nabla_0 R_{n,l}(r) Y_{l,m_l}^*(\hat{r}) \right] \left[ \nabla'_0 R_{n',l'}(r') Y_{l',m_{l'}}^*(\hat{r}') \right] , \end{aligned} \quad (21)$$

where  $\alpha_{n,l,n',l'}^{K,i,f}$  is defined as previously discussed. If we then make use of a relation from Ref. [29],

$$\begin{aligned} \nabla_0 R_{n,l}(r) Y_{l,m_l}^*(\hat{r}) &= \sqrt{\frac{(l+1)^2 - m_l^2}{(2l+1)(2l+3)}} \left( \frac{dR_{n,l}(r)}{dr} - \frac{l}{r} R_{n,l}(r) \right) Y_{l+1,m_l}^*(\hat{r}) \\ &+ \sqrt{\frac{l^2 - m_l^2}{(2l-1)(2l+1)}} \left( \frac{dR_{n,l}(r)}{dr} + \frac{l+1}{r} R_{n,l}(r) \right) Y_{l-1,m_l}^*(\hat{r}), \end{aligned} \quad (22)$$

we can expand our expression into four terms, and then evaluate the individual terms at  $\vec{r} = \vec{r}'$ . This yields the main result of this work,

$$\begin{aligned} \nabla_0 \nabla'_0 \rho(\vec{r}, \vec{r}')|_{\vec{r}=\vec{r}'} &= \sum_{n,l,n',l',K,k,m_l,m_{l'}} \alpha_{n,l,n',l'}^K (l m_l l' m_{l'} | LM) \\ &\times \left[ c_{00} \left( \frac{dR_{n,l}(r)}{dr} - \frac{l}{r} R_{n,l}(r) \right) \left( \frac{dR_{n',l'}(r)}{dr} - \frac{l'}{r} R_{n',l'}(r) \right) \right. \\ &+ c_{01} \left( \frac{dR_{n,l}(r)}{dr} - \frac{l}{r} R_{n,l}(r) \right) \left( \frac{dR_{n',l'}(r)}{dr} + \frac{l'+1}{r} R_{n',l'}(r) \right) \\ &+ c_{02} \left( \frac{dR_{n,l}(r)}{dr} + \frac{l+1}{r} R_{n,l}(r) \right) \left( \frac{dR_{n',l'}(r)}{dr} - \frac{l'}{r} R_{n',l'}(r) \right) \\ &\left. + c_{03} \left( \frac{dR_{n,l}(r)}{dr} + \frac{l+1}{r} R_{n,l}(r) \right) \left( \frac{dR_{n',l'}(r)}{dr} + \frac{l'+1}{r} R_{n',l'}(r) \right) \right] Y_{LM}^*(\hat{r}), \end{aligned} \quad (23)$$

where the products of spherical harmonics have been reduced to single spherical harmonics and then collected under the same index. This allows us to pull all angular behavior outside of the brackets and into a single spherical harmonic,  $Y_{LM}^*(\hat{r})$ . The  $c_{0j}$  coefficients are angular momentum factors, an

example of which is provided below in Eq. (24).

$$c_{00} = \sqrt{\frac{(l+1)^2 - m_l^2}{(2l+1)(2l+3)}} \sqrt{\frac{(l'+1)^2 - m_{l'}^2}{(2l'+1)(2l'+3)}} \sqrt{\frac{(2l+3)(2l'+3)}{4\pi(2L+1)}} \times (l+1 m_l l' + 1 m_{l'} | LM) (l+1 0 l' + 1 0 | L 0) \quad (24)$$

The factors are more complicated for the  $\nabla_{\pm 1} \nabla'_{\mp 1}$  terms, simply due to the  $l$ -projection quantum numbers. Nevertheless, the procedure is identical for the other components.

## 3.0 Analysis

### 3.1 Review of nonlocal density results

In this section, as in Ref. [1], we will briefly discuss results for the nonlocal densities as described in Sec. 2.2.

To showcase the drastic effects of COM removal in light nuclei, we review results for the ground state densities of the  $^{4,6,8}\text{He}$ ,  $^{12}\text{C}$ , and  $^{16}\text{O}$  systems. The translationally invariant (*trinv*) and COM contaminated (*wiCOM*) nonlocal densities are calculated for the aforementioned nuclei according to Eq. (5) and Eq. (3), respectively. All angular dependence factorized out for plotting. Proton densities are shown in blue, neutron densities are shown in red, and total densities will be shown in black. Convergence tests were performed as described in Ref. [1].

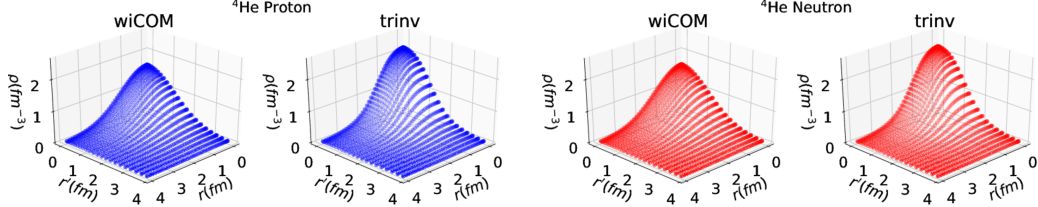


Figure 1: Ground state  $^4\text{He}$  nonlocal proton and neutron densities calculated using the bare NN-N $^4\text{LO}(500)$  interaction with an  $N_{\max} = 18$  basis space. An oscillator frequency of  $\hbar\Omega = 20.0$  MeV was used for this calculation.

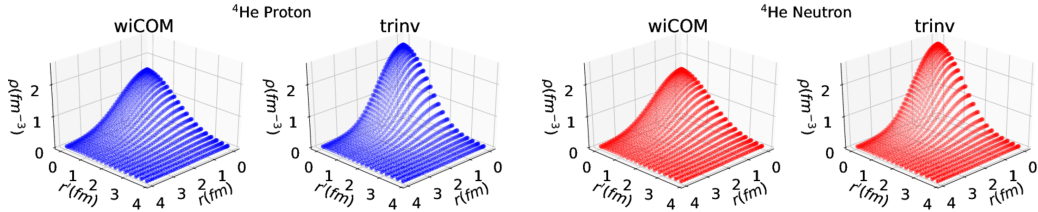


Figure 2: Ground state  $^4\text{He}$  nonlocal proton and neutron densities calculated using the SRG-evolved NN-N $^4\text{LO}(500)$ +3Nlnl interaction with an  $N_{\max} = 14$  basis space. An oscillator frequency of  $\hbar\Omega = 20.0$  MeV and a flow parameter of  $\lambda_{\text{SRG}} = 2.0$  fm $^{-1}$  were used for the calculations.

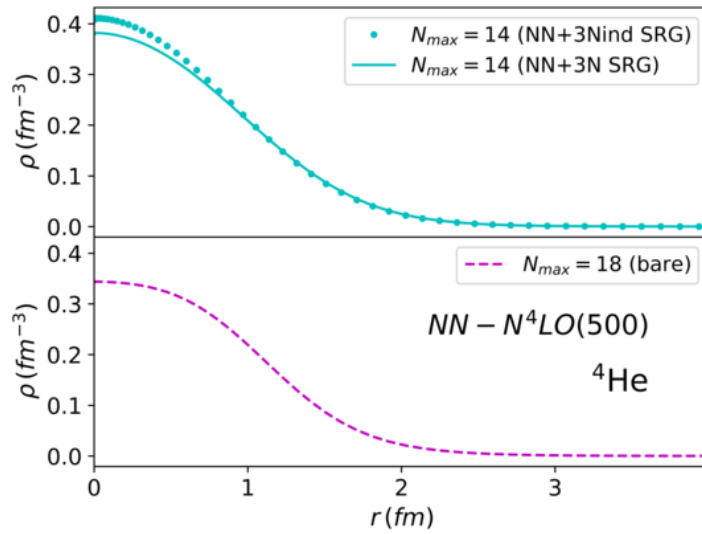


Figure 3: Ground state  $trinv$  local density comparison for  $^4\text{He}$ . In the top panel are calculations with two-body (NN+3Nind SRG) and two- plus three-body (NN+3N SRG) SRG-evolved interactions, while in the bottom panel we have the bare two-body NN-N $^4\text{LO}(500)$  interaction.

Shown in Fig. 1 and Fig. 2 are comparison plots of nonlocal densities with the bare NN-N<sup>4</sup>LO(500) interaction and with the SRG-evolved NN-N<sup>4</sup>LO(500)+3Nnl interaction, respectively. The main difference is that the SRG-evolved interaction includes the full three-body interaction, with all higher order SRG induced terms neglected. We used an  $N_{\max}=18$  and  $N_{\max} = 14$  basis space for the bare and SRG-evolved calculations, respectively. If we consider the differences between the bare and SRG-evolved interactions, we notice slight changes in the predicted nuclear structure. Overall, we notice the features of the bare density tend to be significantly sharper than those of the SRG-evolved interaction. These features are perhaps more noticeable by studying the local density, as shown in Fig. 3. In the top panel, we show the SRG-evolved interaction with just the SRG induced three-body (NN+3Nind SRG) terms and the SRG-evolved interaction with the full chiral three-body interaction (NN+3N SRG). The alterations made by including the full three-body interaction are noticeable, and certainly push the nuclear density much closer to the bare interaction result. As we discuss the results, we will treat the SRG-evolved interaction as its own physically realistic interaction.

Consider Figs. 2, 4, and 5. Here we discuss the results for lighter nuclear systems <sup>4,6,8</sup>He using the NN-N<sup>4</sup>LO(500)+3Nnl potential.  $N_{\max} = 14$ ,  $N_{\max} = 12$ , and  $N_{\max} = 10$  basis spaces were used, respectively, along with a  $\lambda_{\text{SRG}} = 2.0 \text{ fm}^{-1}$  flow parameter and an oscillator frequency of  $\hbar\Omega = 20.0 \text{ MeV}$ . As we know the COM term scales as  $\frac{1}{A}$ , we discuss these nuclei since we expect the COM removal technique to have the largest effect on nuclear structure predictions. One can appreciate the magnitude of difference between the *trinv* and *wiCOM* densities for all nuclei, though as expected, with increasing nucleon number we do observe a decrease in the effects of

COM removal. Nevertheless, we observe sharper features and more rapidly declining edges in the  $trinv$  density. Thus, the COM appears to suppress some of the short range nuclear structure, smoothing it out over larger distances.

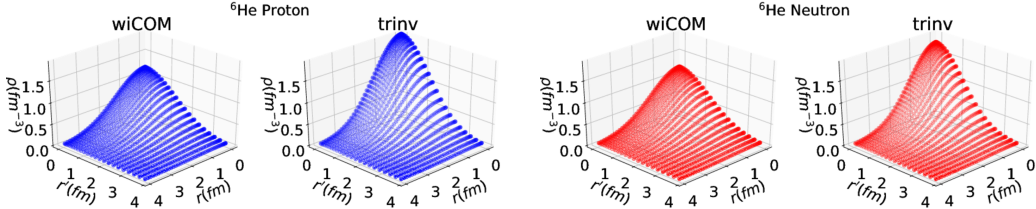


Figure 4: Ground state  $^6\text{He}$  nonlocal proton and neutron densities calculated using the NN-N<sup>4</sup>LO(500)+3Nlnl interaction with an  $N_{\max} = 12$  basis space. An oscillator frequency of  $\hbar\Omega = 20.0$  MeV and a flow parameter of  $\lambda_{\text{SRG}} = 2.0$  fm<sup>-1</sup> were used for the calculations.

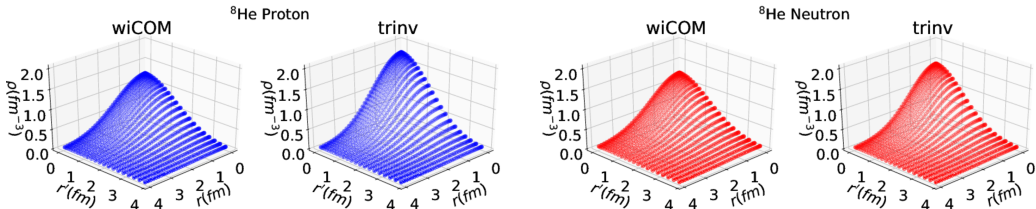


Figure 5: Ground state  $^8\text{He}$  nonlocal proton and neutron densities calculated using the NN-N<sup>4</sup>LO(500)+3Nlnl interaction with an  $N_{\max} = 10$  basis space. An oscillator frequency of  $\hbar\Omega = 20.0$  MeV and a flow parameter of  $\lambda_{\text{SRG}} = 2.0$  fm<sup>-1</sup> were used for the calculations.

Moving to larger systems, we review results in Fig. 6 and Fig. 7 for  $^{12}\text{C}$  and  $^{16}\text{O}$ . As expected, the results of the COM removal procedure are reduced in effect, and are difficult to notice in the nonlocal density plots, especially in comparison to the drastic changes seen in the lighter nuclei considered.

While we have a reduction in peak height differences, we notice the edges of the nuclear density matrix still falling to zero more rapidly than one sees in the COM contaminated density. Moreover, as the kinetic density is dependent on gradients of the nonlocal density, we expect that it may

amplify the effects we are seeing in the density, and so it is still important for us to perform the COM removal on these nuclei, as discussed in Ref. [1].

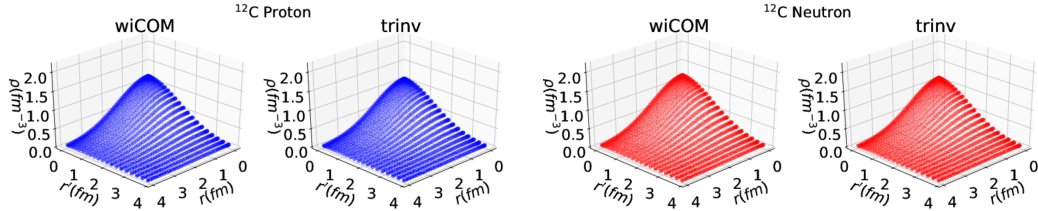


Figure 6: Ground state  $^{12}\text{C}$  nonlocal proton and neutron densities computed using the NN-N<sup>4</sup>LO(500)+3Nlnl interaction with an  $N_{\max} = 8$  importance truncated basis space, an oscillator frequency of  $\hbar\Omega = 20.0$  MeV, and a flow parameter of  $\lambda_{\text{SRG}} = 1.8$  fm $^{-1}$ .

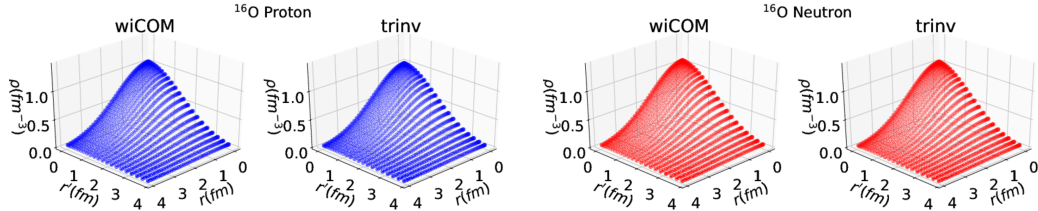


Figure 7: Ground state  $^{16}\text{O}$  nonlocal proton and neutron densities computed using the NN-N<sup>4</sup>LO(500)+3Nlnl interaction with an  $N_{\max} = 8$  importance truncated basis space, an oscillator frequency of  $\hbar\Omega = 20.0$  MeV, and a flow parameter of  $\lambda_{\text{SRG}} = 1.8$  fm $^{-1}$ .

To better illustrate the points discussed above, we present the proton and neutron local densities  $\rho_N(r) = \rho_N(r, r)$  for  $^{4,6,8}\text{He}$ ,  $^{12}\text{C}$ , and  $^{16}\text{O}$  in Figs. 8, 9, 10, 11, and 12, respectively. A noteworthy point about the local densities is that in the larger nuclei, we are able to notice more drastic differences not so easily seen previously. This is another indication that the COM removal procedure is still important in these larger systems, even if it provides only a fine correction to the calculations. Thus, we find that the procedure is still relevant and that we expect noticeable changes in our results for the kinetic density of both  $^{12}\text{C}$  and  $^{16}\text{O}$ .

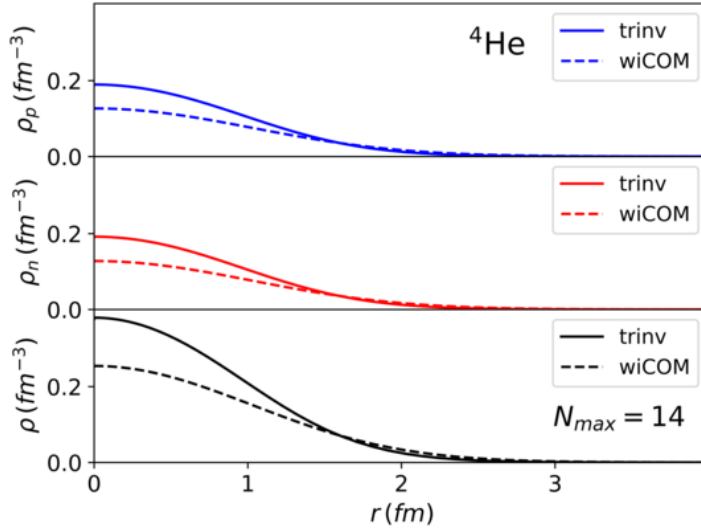


Figure 8: Ground state  $^4\text{He}$  local proton and neutron densities computed using the NN-N<sup>4</sup>LO(500)+3Nlnl interaction with an  $N_{\max} = 14$  basis space, an oscillator frequency of  $\hbar\Omega = 20.0$  MeV, and a flow parameter of  $\lambda_{\text{SRG}} = 2.0$  fm<sup>-1</sup>.

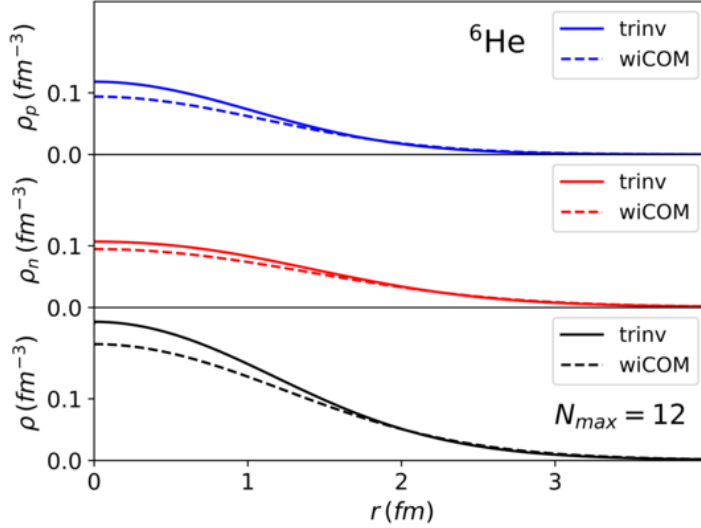


Figure 9: Ground state  $^6\text{He}$  local proton and neutron densities computed using the NN-N<sup>4</sup>LO(500)+3Nlnl interaction with an  $N_{\max} = 12$  basis space, an oscillator frequency of  $\hbar\Omega = 20.0$  MeV, and a flow parameter of  $\lambda_{\text{SRG}} = 2.0$  fm<sup>-1</sup>.

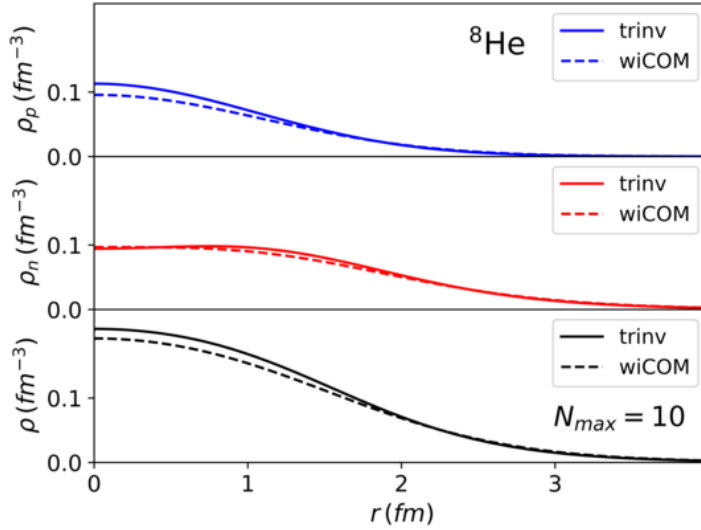


Figure 10: Ground state  ${}^8\text{He}$  local proton and neutron densities computed using the NN-N<sup>4</sup>LO(500)+3Nlnl interaction with an  $N_{\max} = 10$  basis space, an oscillator frequency of  $\hbar\Omega = 20.0$  MeV, and a flow parameter of  $\lambda_{\text{SRG}} = 2.0$  fm<sup>-1</sup>.

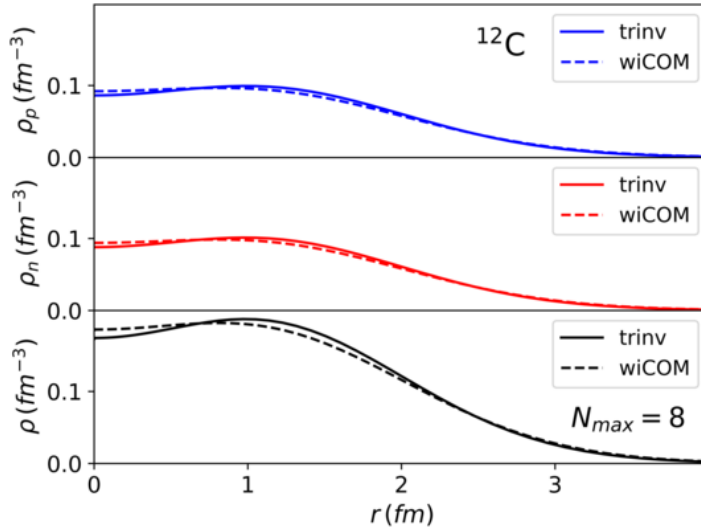


Figure 11: Ground state  ${}^{12}\text{C}$  local proton and neutron densities computed using the NN-N<sup>4</sup>LO(500)+3Nlnl interaction with an  $N_{\max} = 10$  basis space, an oscillator frequency of  $\hbar\Omega = 20.0$  MeV, and a flow parameter of  $\lambda_{\text{SRG}} = 2.0$  fm<sup>-1</sup>.

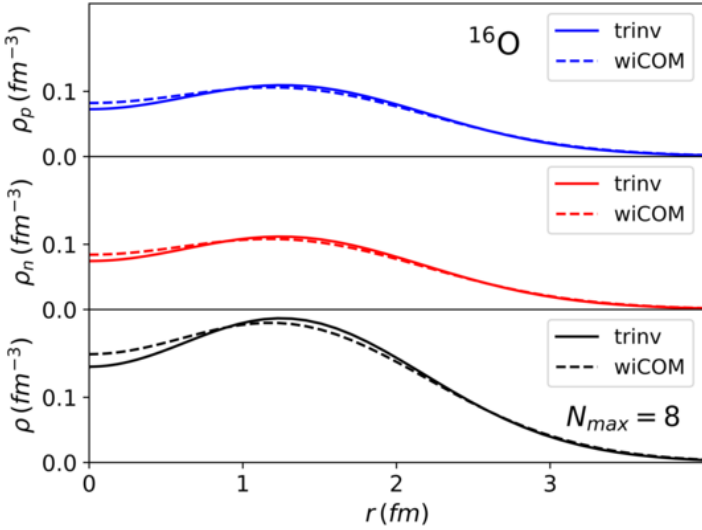


Figure 12: Ground state  $^{16}\text{O}$  local proton and neutron densities computed using the NN-N<sup>4</sup>LO(500)+3Nlnl interaction with an  $N_{\max} = 10$  basis space, an oscillator frequency of  $\hbar\Omega = 20.0$  MeV, and a flow parameter of  $\lambda_{\text{SRG}} = 2.0$  fm<sup>-1</sup>.

### 3.2 Kinetic density results

In this section we discuss the main results of this work; the nuclear kinetic density calculated from the *ab initio* NCSM nonlocal densities. These results have been submitted for publishing and are available for additional review on arXiv:1808.10537. We discuss results for all aforementioned nuclei, however it should be noted that the only reasonable comparison to a many-body method such as DFT can be made with  $^{16}\text{O}$ . Proton kinetic densities are shown in blue, neutron kinetic densities are shown in red, and the total kinetic density is shown in black. Convergence tests were performed as described in Ref. [1].

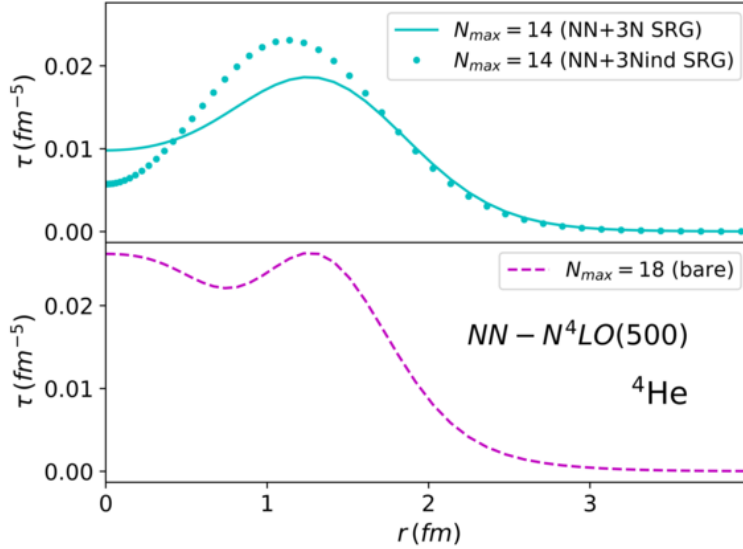


Figure 13: Ground state *trinv* kinetic density comparison for  ${}^4\text{He}$ . In the top panel are calculations with two-body (NN+3Nind SRG) and two- plus three- body (NN+3N SRG) SRG-evolved interactions, while in the bottom panel we have the bare two-body NN- $N^4\text{LO}(500)$  interaction. Nonlocal densities were computed as previously described in Fig. 1 and Fig. 2, respectively.

As before, we initially discuss results for the SRG-evolved and bare interactions as applied to  ${}^4\text{He}$ . In the Fig. 13 top panel, we show kinetic density results using the SRG-evolved two-body interaction including induced three-body terms (NN+3Nind SRG) and also the full chiral two- plus three-nucleon interactions (NN+3N SRG). In the bottom panel, we show the kinetic density results computed from the bare interaction. Notably, the structural differences in the kinetic density are significant for less than one fermi when compared to the corresponding differences observed in the nuclear densities. This emphasizes how sensitive the kinetic density is to the nuclear structure. Once again, going forward we will act as though the SRG-evolved interaction is its own physically realistic interaction.

Beginning with the lighter nuclei, consider the plots of the nuclear kinetic

density shown in Figs. 14, 15, and 16, with the nonlocal densities calculated as previously described in Sec. 3.1. The kinetic density results for these light systems best illustrate how the COM removal procedure impacts objects dependent on the nonlocal density. The remarkable difference in the predicted short-range structure for the small  $A$ -nucleon systems with the *trinv* and *wiCOM* kinetic densities details precisely why the COM removal procedure is important when attempting to describe light nuclei. The amplification caused by the application of the gradients is quite pronounced, again emphasizing the suppression that is caused by the ground state COM wave function. A behavior similar to that seen in the densities is observed in the COM contaminated kinetic density. Notice that in more exotic nuclei such as  $^{6,8}\text{He}$ , we see pronounced differences in the long-range behavior of the kinetic density as well.

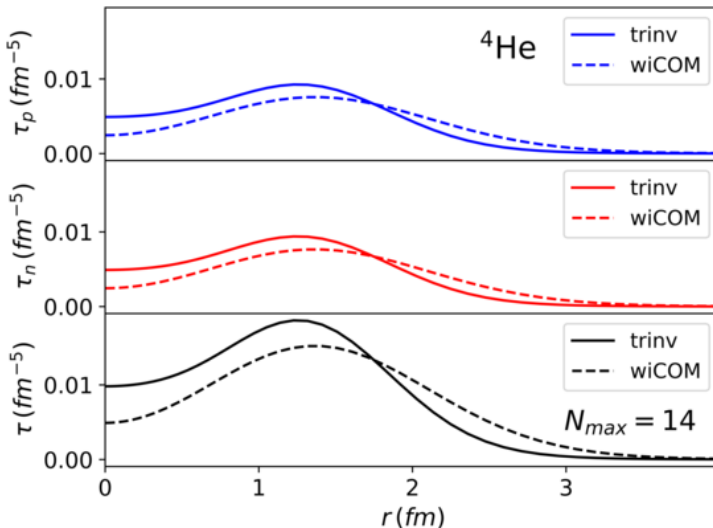


Figure 14: Ground state  $^4\text{He}$  comparisons between the *trinv* and *wiCOM* kinetic densities. The nonlocal density was computed as previously described in Sec. 3.1. The expectation value of the intrinsic kinetic energy for  $^4\text{He}$  is 51.91 MeV.

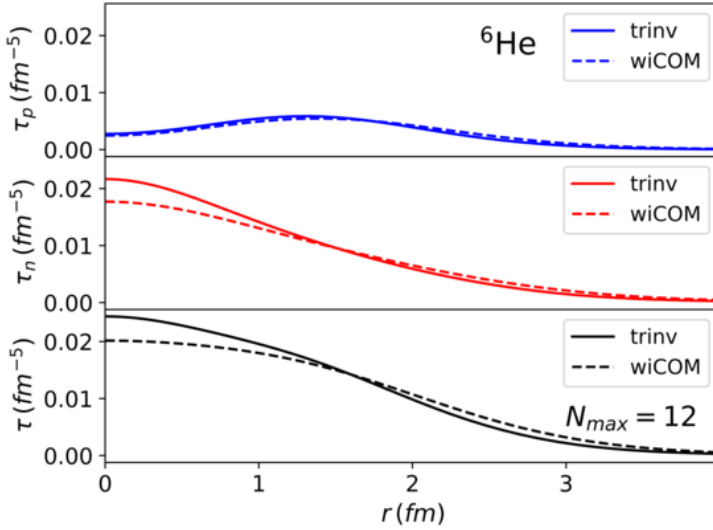


Figure 15: Ground state  ${}^6\text{He}$  comparisons between the *trinv* and *wiCOM* kinetic densities. The nonlocal density was computed as previously described in Sec. 3.1. The expectation value of the intrinsic kinetic energy for  ${}^6\text{He}$  is 78.26 MeV.

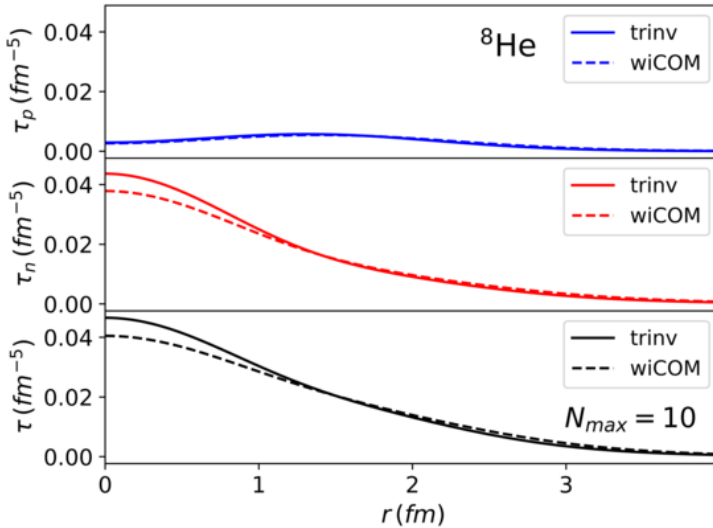


Figure 16: Ground state  ${}^8\text{He}$  comparisons between the *trinv* and *wiCOM* kinetic densities. The nonlocal density was computed as previously described in Sec. 3.1. The expectation value of the intrinsic kinetic energy for  ${}^8\text{He}$  is 116.30 MeV.

If we now look to the kinetic densities of heavier  $A$ -nucleon systems shown in

Figs. 17 and 18, we may attempt to directly compare the effects of COM contamination in the energy functionals of DFT. The nonlocal densities were computed as previously described in Sec. 3.1, with importance truncated NCSM basis spaces. While we do see the expected suppression from the COM contamination in the kinetic density, the effects are not nearly as pronounced as we expected them to be given the effects seen in the lighter systems. In both systems, we observe drastically reduced effects from the COM removal process, which may be in part due to the highly spherical shape of a system like  $^{16}\text{O}$ , however this requires a deeper investigation. Nevertheless, the *trinv* and *wiCOM* nuclear densities produce non-negligible alterations in the kinetic density, which have the opportunity to provide fine structure corrections if used as an input in energy density functionals.

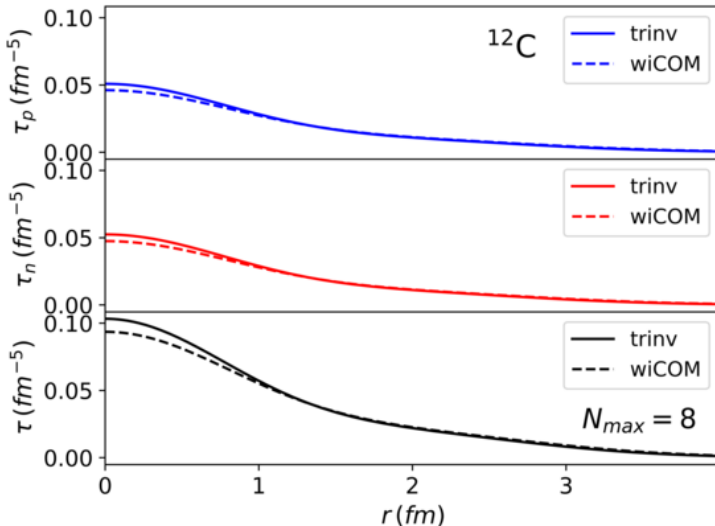


Figure 17: Ground state  $^{12}\text{C}$  comparisons between the *trinv* and *wiCOM* kinetic densities. The nonlocal density was computed as previously described in Sec. 3.1. The expectation value of the intrinsic kinetic energy for  $^{12}\text{C}$  is 219.84 MeV.

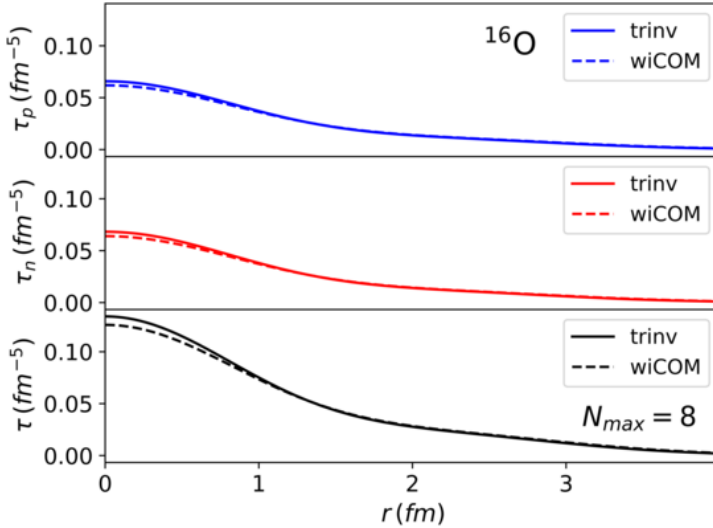


Figure 18: Ground state  $^{16}\text{O}$  comparisons between the *trinv* and *wiCOM* kinetic densities. The nonlocal density was computed as previously described in Sec. 3.1. The expectation value of the intrinsic kinetic energy for  $^{16}\text{O}$  is 301.69 MeV.

As confirmation of the success of the COM removal procedure, we bring the discussion to the integration of the coordinate space kinetic density. In the following NCSM states, note that we only consider the  $J = 0$  contribution since we present results only for the ground-state of the aforementioned nuclei. When considering the *trinv* kinetic density, integration over all space returns the exact expectation value of the ground state intrinsic kinetic energy operator for each nucleus. The mean value intrinsic kinetic energy is independently calculated according to the two-body density matrix elements, introduced in second quantization, according to

$$\langle T_{int} \rangle = \frac{1}{4} \sum_{abcd} \langle ab | T_{int} | cd \rangle_{SD} \langle A\lambda JT | a_a^\dagger a_b^\dagger a_d a_c | A\lambda JT \rangle_{SD}. \quad (25)$$

When performing the integration with the COM contaminated kinetic density, one exactly recovers the expectation value of the intrinsic kinetic

Nucleus	$N_{\max}$	$\langle T_{int} \rangle$	Error ( $\pm$ )
$^4\text{He}$ (bare)	18	62.73	$\pm 0.01 \%$
$^4\text{He}$	14	51.91	$\pm 0.01 \%$
$^6\text{He}$	12	78.26	$\pm 1.4 \%$
$^8\text{He}$	10	116.30	$\pm 3.1 \%$
$^{12}\text{C}$	8 IT	219.84	$\pm 1.2 \%$
$^{16}\text{O}$	8 IT	301.69	$\pm 0.8 \%$

Table 1: Ground state mean intrinsic kinetic energy values and percent errors for all aforementioned nuclei calculated using the NN-N<sup>4</sup>LO(500)+3Nlnl interaction (except  $^4\text{He}$ -bare, which are the results for the bare NN-N<sup>4</sup>LO(500) interaction). All  $\langle T_{int} \rangle$  values are in MeV. Note *IT* refers to an importance truncated basis space. Error is calculated using the percent difference between the maximum  $N_{\max}$  value and the previous value.

energy operator in addition to the expectation value of the mean value COM kinetic energy. The contribution of the ground state COM wave function is equivalent to  $\frac{3}{4}\hbar\Omega$ . The recovery of the expectation value of the intrinsic kinetic energy operator is direct confirmation of the success of the COM removal procedure. The results for the mean value kinetic energy operator are summarized in Table 1. The set of relations describing these observations are:

$$\begin{aligned}
\langle T_{wiCOM} \rangle &= {}_{SD} \langle A\lambda JT | \tau_0^{wiCOM} | A\lambda JT \rangle {}_{SD} \\
&= \frac{\hbar^2}{2m} \int_0^\infty r^2 \tau_0^{wiCOM}(r) dr \\
&= {}_{SD} \langle A\lambda JT | \tau_0^{int} + \tau_0^{COM} | A\lambda JT \rangle {}_{SD} \\
&= \langle T_{int} \rangle + \frac{3}{4}\hbar\Omega ,
\end{aligned} \tag{26}$$

$$\begin{aligned}
\langle T_{int} \rangle &= \langle T_{wiCOM} \rangle - \frac{3}{4} \hbar \Omega \\
&= {}_{SD} \langle A \lambda J T | \tau_0^{trinv} | A \lambda J T \rangle {}_{SD} \\
&= \frac{\hbar^2}{2m} \int_0^\infty r^2 \tau_0^{trinv}(r) dr ,
\end{aligned} \tag{27}$$

where  $m$  is the nucleon mass and  $\tau_0$  is the total kinetic density.

### 3.3 Comparison to basic DFT calculation

Recall the form of Eq. (8). The contribution to the local energy density of this term has no treatment for the COM contamination. However, according to Ref. [30], a basic COM removal treatment can be introduced in DFT as:

$$\mathcal{H}_{kinetic}(\vec{r}) = \frac{\hbar^2}{2m} \left(1 - \frac{1}{A}\right) \tau_0(\vec{r}), \tag{28}$$

where we have a term inversely proportional the nucleon number being subtracted from the standard kinetic term  $\tau_0$ , which would be  $\tau_{wiCOM}$  in our calculations. We will label this kinetic density as follows,

$$\tau_{DFT}(\vec{r}) = \left(1 - \frac{1}{A}\right) \tau_{wiCOM}(\vec{r}). \tag{29}$$

In Fig. 19, we show all three calculations – *trinv*, *wiCOM*, and DFT – of the kinetic density for  ${}^{4,8}\text{He}$ ,  ${}^{12}\text{C}$ , and  ${}^{16}\text{O}$ . A most noteworthy feature of the plots is the differences between the DFT and the *ab initio trinv* kinetic density curves. The mock DFT calculation has reduced the overall size of the kinetic density curve, quite drastically in lighter nuclei. In particular, the short-range behavior is pushed further from the *ab initio* calculations, whereas the long-range behavior is actually pushed closer. In fact, if we are to imagine this mock calculation as being accurate, the differences between

the *ab initio* kinetic density and DFT kinetic density will be more pronounced than previously thought, even in the larger  $A$ -nucleon systems.

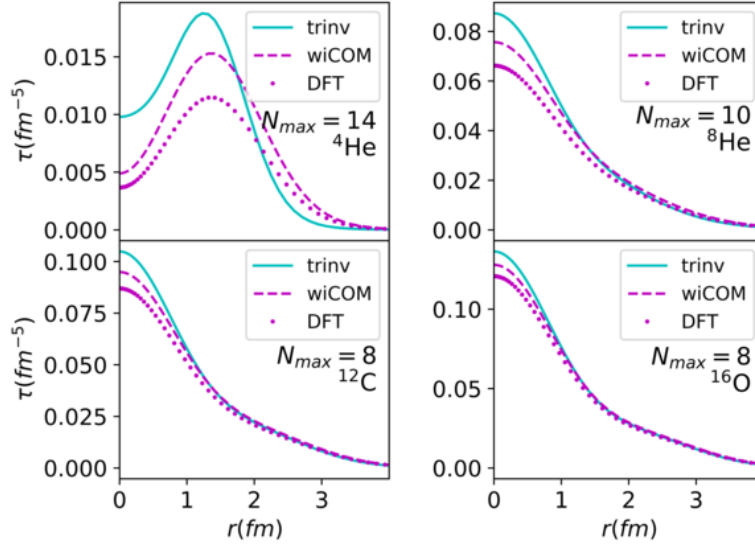


Figure 19: Ground state kinetic density results for  $^{4,8}\text{He}$ ,  $^{12}\text{C}$ , and  $^{16}\text{O}$  calculated with the NN-N<sup>4</sup>LO(500)+3Nlnl interaction. The nonlocal densities for the nuclei were computed as previously described in Sec. 3.1. The DFT kinetic density was obtained by using Eq. (29),  $\tau_{DFT}(r) = (1 - \frac{1}{A})\tau_{wiCOM}(r)$ .

In the following table, we show results for the expectation value of the kinetic energy operator for all three kinetic densities – *trinv*, *wiCOM*, and DFT. Comparing values across columns, we find that both COM removal techniques produce surprisingly agreeable mean values with the  $\langle T_{DFT} \rangle$  consistently slightly underestimating the true mean value. This is particularly surprising given the structural differences in the predicted kinetic density. The mock DFT calculations has reduced the integral value appropriately, in essence removing COM contamination from the mean value, however the structure produced is highly irregular in comparison to the *ab initio* calculation.

Nucleus	$N_{\max}$	$\langle T_{int} \rangle$	$\langle T_{wiCOM} \rangle$	$\langle T_{DFT} \rangle$
$^4\text{He}$	14	51.91	66.91	50.18
$^6\text{He}$	12	78.26	93.26	77.72
$^8\text{He}$	10	116.30	131.30	114.89
$^{12}\text{C}$	8 IT	219.84	234.84	215.27
$^{16}\text{O}$	8 IT	301.69	316.69	296.90

Table 2: Ground state mean intrinsic kinetic energy values using *trinv*, *wiCOM*, and DFT kinetic densities for all aforementioned nuclei, calculated with the NN-N<sup>4</sup>LO(500)+3Nlnl interaction. All  $\langle T_i \rangle$  values are in MeV. Note *IT* refers to an importance truncated basis space. The  $\langle T_{DFT} \rangle$  is calculated by using Eq. (29),  $\langle T_{DFT} \rangle = (1 - \frac{1}{A})\langle T_{wiCOM} \rangle$ .

## 4.0 Conclusions

The main goal of this work was to provide an *ab initio* connection to DFT through the nuclear kinetic density, such that it is possible to make comparisons between COM removal procedures in the different many-body methods. An *ab initio* construction of the nonlocal one-body densities according to Ref. [1] allows us to derive an analytic formula relating the kinetic density to the nuclear density, the procedure for which is outlined in Sec. 2.3. The nonlocal densities are computed from the many-body wave functions calculated in the NCSM approach. In Sec. 3.1, we reviewed results for the nonlocal translationally invariant and COM contaminated one-body nuclear density for the  $^{4,6,8}\text{He}$ ,  $^{12}\text{C}$ , and  $^{16}\text{O}$  systems. The nuclear density results, and hence the obtained kinetic density results, were generated using the SRG-evolved NN-N<sup>4</sup>LO(500)+3Nlnl chiral interaction [1, 22]. As illustrated in Sec. 3.2, the procedure for COM removal inflicts non-negligible changes to the structure of the kinetic density, as expected from the review of the COM removal being applied to the nonlocal densities. In Sec. 3.3, we used a COM treatment from DFT in the kinetic density contribution to the local energy density functional, allowing us to compare the *trinv* kinetic density to a mock DFT kinetic density. Interestingly, we found that the mean value kinetic energy of the nuclei agreed well across both COM removal techniques, however the predicted DFT structure of the kinetic density differed quite heavily from the *ab initio* calculations, especially in the short-range behavior.

In conclusion, the previous construction of a general nonlocal density allowed for the proper computation of objects dependent on the nuclear density, such as the kinetic density. This provides a bridge for communities to gauge

differences in COM removal procedures across various many-body techniques. While the effects of COM removal are generally not as drastic in larger  $A$ -nucleon systems, the effects are non-negligible and should motivate the need to procedurally remove spurious COM contamination, or at the very least motivate the need to check existing methods for COM removal.

## 5.0 Recommendations

It is recommended that all calculations involving light- to medium-mass nuclei utilize the nonlocal translationally invariant density, or utilize more adept COM removal procedures, when constructing quantities dependent on the nuclear density. It is further recommended that additional comparisons to DFT be made using *ab initio* many-body methods, such that COM removal procedures may be better studied and fine corrections may be added to DFT calculations.

## 6.0 Appendix

### 6.1 Kinetic density coefficients

This section contains all  $c_{ij}$  coefficients of the kinetic density terms. Note that  $\pm$  or  $\mp$  indicates the order of application of the  $\nabla$  operators.

$$c_{00} = \sqrt{\frac{(l+1)^2 - m_l^2}{(2l+1)(2l+3)}} \sqrt{\frac{(l'+1)^2 - m_{l'}^2}{(2l'+1)(2l'+3)}} \sqrt{\frac{(2l+3)(2l'+3)}{4\pi(2L+1)}} \quad (30)$$

$$\times (l+1 m_l l' + 1 m_{l'} | LM) (l+1 0 l' + 1 0 | L 0)$$

$$c_{01} = \sqrt{\frac{(l+1)^2 - m_l^2}{(2l+1)(2l+3)}} \sqrt{\frac{l'^2 - m_{l'}^2}{(2l'-1)(2l'+1)}} \sqrt{\frac{(2l+3)(2l'-1)}{4\pi(2L+1)}} \quad (31)$$

$$\times (l+1 m_l l' - 1 m_{l'} | LM) (l+1 0 l' - 1 0 | L 0)$$

$$c_{02} = \sqrt{\frac{l^2 - m_l^2}{(2l-1)(2l+1)}} \sqrt{\frac{(l'+1)^2 - m_{l'}^2}{(2l'+1)(2l'+3)}} \sqrt{\frac{(2l-1)(2l'+3)}{4\pi(2L+1)}} \quad (32)$$

$$\times (l-1 m_l l' + 1 m_{l'} | LM) (l-1 0 l' + 1 0 | L 0)$$

$$c_{02} = \sqrt{\frac{l^2 - m_l^2}{(2l-1)(2l+1)}} \sqrt{\frac{l'^2 - m_{l'}^2}{(2l'-1)(2l'+1)}} \sqrt{\frac{(2l-1)(2l'-1)}{4\pi(2L+1)}} \quad (33)$$

$$\times (l-1 m_l l' - 1 m_{l'} | LM) (l-1 0 l' - 1 0 | L 0)$$

$$c_{\pm 10} = \sqrt{\frac{(l+m_l+1)(l+m_l+2)}{2(2l+1)(2l+3)}} \sqrt{\frac{(l'-m_{l'}+1)(l'-m_{l'}+2)}{2(2l'+1)(2l'+3)}} \sqrt{\frac{(2l+3)(2l'+3)}{4\pi(2L+1)}} \quad (34)$$

$$\times (l+1 m_l + 1 l' + 1 m_{l'} - 1 | LM) (l+1 0 l' + 1 0 | L 0)$$

$$\begin{aligned}
c_{\pm 11} = & -\sqrt{\frac{(l+m_l+1)(l+m_l+2)}{2(2l+1)(2l+3)}} \sqrt{\frac{(l'+m_{l'}-1)(l'+m_{l'})}{2(2l'-1)(2l'+1)}} \sqrt{\frac{(2l+3)(2l'-1)}{4\pi(2L+1)}} \\
& \times (l+1 m_l + 1 l' - 1 m_{l'} - 1 | LM) (l+1 0 l' - 1 0 | L 0)
\end{aligned} \tag{35}$$

$$\begin{aligned}
c_{\pm 12} = & -\sqrt{\frac{(l-m_l-1)(l-m_l)}{2(2l-1)(2l+1)}} \sqrt{\frac{(l'-m_{l'}+1)(l'-m_{l'}+2)}{2(2l'+1)(2l'+3)}} \sqrt{\frac{(2l-1)(2l'+3)}{4\pi(2L+1)}} \\
& \times (l-1 m_l + 1 l' + 1 m_{l'} - 1 | LM) (l-1 0 l' + 1 0 | L 0)
\end{aligned} \tag{36}$$

$$\begin{aligned}
c_{\pm 13} = & \sqrt{\frac{(l-m_l-1)(l-m_l)}{2(2l-1)(2l+1)}} \sqrt{\frac{(l'+m_{l'}-1)(l'+m_{l'})}{2(2l'-1)(2l'+1)}} \sqrt{\frac{(2l-1)(2l'-1)}{4\pi(2L+1)}} \\
& \times (l-1 m_l + 1 l' - 1 m_{l'} - 1 | LM) (l-1 0 l' - 1 0 | L 0)
\end{aligned} \tag{37}$$

$$\begin{aligned}
c_{\mp 10} = & \sqrt{\frac{(l-m_l+1)(l-m_l+2)}{2(2l+1)(2l+3)}} \sqrt{\frac{(l'+m_{l'}+1)(l'+m_{l'}+2)}{2(2l'+1)(2l'+3)}} \sqrt{\frac{(2l+3)(2l'+3)}{4\pi(2L+1)}} \\
& \times (l+1 m_l - 1 l' + 1 m_{l'} + 1 | LM) (l+1 0 l' + 1 0 | L 0)
\end{aligned} \tag{38}$$

$$c_{\mp 11} = -\sqrt{\frac{(l-m_l+1)(l-m_l+2)}{2(2l+1)(2l+3)}} \sqrt{\frac{(l'-m_{l'}-1)(l'-m_{l'})}{2(2l'-1)(2l'+1)}} \sqrt{\frac{(2l+3)(2l'-1)}{4\pi(2L+1)}} \\ \times (l+1 m_l - 1 l' - 1 m_{l'} + 1 | LM) (l+1 0 l' - 1 0 | L 0) \\ (39)$$

$$c_{\mp 12} = -\sqrt{\frac{(l+m_l-1)(l+m_l)}{2(2l-1)(2l+1)}} \sqrt{\frac{(l'+m_{l'}+1)(l'+m_{l'}+2)}{2(2l'+1)(2l'+3)}} \sqrt{\frac{(2l-1)(2l'+3)}{4\pi(2L+1)}} \\ \times (l-1 m_l - 1 l' + 1 m_{l'} + 1 | LM) (l-1 0 l' + 1 0 | L 0) \\ (40)$$

$$c_{\mp 13} = \sqrt{\frac{(l+m_l-1)(l+m_l)}{2(2l-1)(2l+1)}} \sqrt{\frac{(l'-m_{l'}-1)(l'-m_{l'})}{2(2l'-1)(2l'+1)}} \sqrt{\frac{(2l-1)(2l'-1)}{4\pi(2L+1)}} \\ \times (l-1 m_l - 1 l' - 1 m_{l'} + 1 | LM) (l-1 0 l' - 1 0 | L 0) \\ (41)$$

## 7.0 Acknowledgments

We would like to acknowledge Angelo Calci for useful discussions and Witek Nazarewicz for helpful comments on this work. This work was supported by the NSERC Grant No. SAPIN-2016-00033. TRIUMF receives federal funding via a contribution agreement with the National Research Council of Canada. Computing support came from an INCITE Award on the Titan supercomputer of the Oak Ridge Leadership Computing Facility (OLCF) at ORNL, from Calcul Quebec, Westgrid and Compute Canada.

## References

- [1] M. Gennari, M. Vorabbi, A. Calci, and P. Navrátil, “Microscopic optical potentials derived from ab initio translationally invariant nonlocal one-body densities,” *Physical Review C*, vol. 97, no. 3, p. 034619, 2018.
- [2] B. R. Barrett, P. Navrátil, and J. P. Vary, “Ab initio no core shell model,” *Progress in Particle and Nuclear Physics*, vol. 69, pp. 131–181, 2013.
- [3] T. Duguet, “The nuclear energy density functional formalism,” in *The Euroschool on Exotic Beams, Vol. IV*, pp. 293–350, Springer, 2014.
- [4] D. Vautherin and D. M. Brink, “Hartree-fock calculations with skyrme’s interaction,” *Physics Letters B*, vol. 32, no. 3, pp. 149–153, 1970.
- [5] D. Vautherin and D. t. Brink, “Hartree-fock calculations with skyrme’s interaction. i. spherical nuclei,” *Physical Review C*, vol. 5, no. 3, p. 626, 1972.
- [6] D. Vautherin, “Hartree-fock calculations with skyrme’s interaction. ii. axially deformed nuclei,” *Physical Review C*, vol. 7, no. 1, p. 296, 1973.
- [7] R. G. Parr and W. Yang, “Density-functional theory of atoms and molecules, vol. 16 of international series of monographs on chemistry,” 1989.
- [8] E. K. Gross and R. M. Dreizler, *Density functional theory*, vol. 337. Springer Science & Business Media, 2013.
- [9] A. Bhattacharyya and R. Furnstahl, “The kinetic energy density in

- kohn–sham density functional theory,” *Nuclear Physics A*, vol. 747, no. 2-4, pp. 268–294, 2005.
- [10] F. Hofmann and H. Lenske *Phys. Rev. C*, vol. 57, p. 2281, 1998.
- [11] J. Erler, N. Birge, M. Kortelainen, W. Nazarewicz, E. Olsen, A. M. Perhac, and M. Stoitsov, “The limits of the nuclear landscape,” *Nature*, vol. 486, no. 7404, p. 509, 2012.
- [12] M. Kortelainen, T. Lesinski, J. Moré, W. Nazarewicz, J. Sarich, N. Schunck, M. Stoitsov, and S. Wild, “Nuclear energy density optimization,” *Physical Review C*, vol. 82, no. 2, p. 024313, 2010.
- [13] M. Kortelainen, J. McDonnell, W. Nazarewicz, P.-G. Reinhard, J. Sarich, N. Schunck, M. Stoitsov, and S. Wild, “Nuclear energy density optimization: Large deformations,” *Physical Review C*, vol. 85, no. 2, p. 024304, 2012.
- [14] M. Kortelainen, J. McDonnell, W. Nazarewicz, E. Olsen, P.-G. Reinhard, J. Sarich, N. Schunck, S. Wild, D. Davesne, J. Erler, *et al.*, “Nuclear energy density optimization: Shell structure,” *Physical Review C*, vol. 89, no. 5, p. 054314, 2014.
- [15] F. Wegner *Ann. Phys.*, vol. 506, p. 77, 1994.
- [16] S. Bogner, R. Furnstahl, and R. Perry, “Similarity renormalization group for nucleon-nucleon interactions,” *Physical Review C*, vol. 75, no. 6, p. 061001, 2007.
- [17] R. Roth, S. Reinhardt, and H. Hergert, “Unitary correlation operator method and similarity renormalization group: Connections and

differences,” *Physical Review C*, vol. 77, no. 6, p. 064003, 2008.

- [18] S. Bogner, R. Furnstahll, and A. Schwenk *Program of Particle and Nuclear Physics*, vol. 65, p. 94, 2010.
- [19] E. Jurgenson, P. Navratil, and R. Furnstahl, “Evolution of nuclear many-body forces with the similarity renormalization group,” *Physical review letters*, vol. 103, no. 8, p. 082501, 2009.
- [20] D. Entem, N. Kaiser, R. Machleidt, and Y. Nosyk, “Peripheral nucleon-nucleon scattering at fifth order of chiral perturbation theory,” *Physical Review C*, vol. 91, no. 1, p. 014002, 2015.
- [21] D. Entem, R. Machleidt, and Y. Nosyk *Phys. Rev. C*, vol. 96, p. 024004, 2017.
- [22] P. Navratil, “Local three-nucleon interaction from chiral effective field theory,” *Few-Body Systems*, vol. 41, no. 3-4, pp. 117–140, 2007.
- [23] R. Roth and P. Navrátil, “Ab initio study of  $^{40}\text{Ca}$  with an importance-truncated no-core shell model,” *Phys. Rev. Lett.*, vol. 99, p. 092501, Aug 2007.
- [24] R. Roth, “Importance truncation for large-scale configuration interaction approaches,” *Phys. Rev. C*, vol. 79, p. 064324, Jun 2009.
- [25] P. Navrátil, “Translationally invariant density,” *Physical Review C*, vol. 70, no. 1, p. 014317, 2004.
- [26] L. Trlifaj, “Simple formula for the general oscillator brackets,” *Physical Review C*, vol. 5, no. 5, p. 1534, 1972.

- [27] P. J. Borycki, J. Dobaczewski, W. Nazarewicz, and M. V. Stoitsov, “Pairing renormalization and regularization within the local density approximation,” *Phys. Rev. C*, vol. 73, p. 044319, Apr 2006.
- [28] J. Dobaczewski and J. Dudek, “Time-odd components in the mean field of rotating superdeformed nuclei,” *Physical Review C*, vol. 52, no. 4, p. 1827, 1995.
- [29] D. Varshalovich, A. Moskalev, and V. Khersonskii, *Quantum Theory of Angular Momentum*. World Scientific Pub., 1988.
- [30] J. Dobaczewski, W. Nazarewicz, and M. V. Stoitsov, “Nuclear ground-state properties from mean-field calculations,” in *Exotic Nuclei and Atomic Masses* (J. Åystö, P. Dendooven, A. Jokinen, and M. Leino, eds.), (Berlin, Heidelberg), pp. 55–60, Springer Berlin Heidelberg, 2003.